2025-2 | 50th congress of the Société de Biomécanique
27-29 October 2025, Marseille, France

Multidisciplinary Biomechanics Journal

Evaluation of image quality parameters in lung using MR elastography technique

Philippe Pouletaut[a], Fabrice Charleux[b], Sabine F. Bensamoun[a*]

a Université de technologie de Compiègne, CNRS, BMBI, UMR7338, Compiègne, France
b ACRIM-Polyclinique Saint Côme, Radiology department, Compiègne, France
* Corresponding author: sabine.bensamoun@utc.fr

Received date: 04/04/2025
Accepted date: 27/06/2025
Publication date: 27/10/2025

Keywords: image quality assessment, magnetic resonance elastography, signal-to-noise ratio, lung stiffness

© 2025 The Authors
Licence CC-BY 4.0
Published by Société de Biomécanique

1. Introduction

In clinical practice, lung tissue examination is typically performed using computed tomography (CT), which provides morphological and structural information. Recent studies have shown that even when lung tissue appears structurally normal, without visible infiltrated fibrotic tissue that may induce bronchitis symptoms or signs of emphysema, its stiffness may still be altered (Chakouch et al. 2023).

This stiffness can be quantified using a non-invasive imaging technique called magnetic resonance elastography (MRE). Once the MRE protocol was deemed sufficiently repeatable and reproducible, it was then applied to the monitoring of the lung stiffness in long COVID patients (Bensamoun et al. 2025a) as well as the diagnosis of lung disease caused by tobacco use (Bensamoun et al. 2025b).

While these recent MRE studies have demonstrated that this technique can provide a new imaging biomarker, further development of the MRE lung protocol is necessary. A key aspect of this development is ensuring image quality, which requires evaluating (1) the signal-to-noise ratio (SNR) in MRE magnitude images and (2) the signal quality in stiffness images.

2. Methods

2.1 Recruitment of smoking patients

A cohort of thirty-four smokers referred for a lung CT test was recruited (#A01496-33) at the radiology department (ACRIM) of the Saint Côme Polyclinic (Compiègne). CT scans were analyzed by a senior radiologist, focusing particularly on structural properties such as bronchial thickness, opacities, etc.

2.2 CT, MRI, and MRE image acquisitions

From the CT images, the slice level where the intermediate trunk exhibited a clover-shaped appearance was identified for subsequent MRE assessment in the same lung region. Next, lung density measurement from MRI, acquired using a fast gradient-echo sequence, was calibrated with a Gadolinium-doped water phantom placed on the sternum. MRE test (Fig. 1a) was made using a 1.5 T MRI over a 22 s acquisition. A driver was positioned on the right lung, to avoid heart artefacts, and inducing mechanical shear waves at 50 Hz. A spin-echo echo-planar sequence with motion-encoding gradient was applied to capture shear wave displacement and assess lung stiffness. Data were recorded from 4 axial slices, evenly spaced 15 mm apart, and labeled "Slice 1 to 4" from the upper to the lower level of the patient. Lung stiffness maps were generated from phase and magnitude images using multimodel direct inversion (Silva et al. 2015) and were subsequently corrected for lung density (Bensamoun et al. 2025a).

2.3 Magnitude and phase images analysis

The quality of the MRE magnitude images (Fig. 1b) was assessed by computing the signal-to-noise ratio (SNR).

To cite this article: Philippe Pouletaut, Fabrice Charleux, Sabine F. Bensamoun, Evaluation of image quality parameters in lung using MR elastography technique, *Multidisciplinary Biomechanics Journal*, 2025, vol. 2, p. 115–117, DOI: 10.46298/mbj.16134.

The mean signal intensity (m) was measured in the right lung (RL) contoured by a red profile, while the noise, corresponding to the standard deviation (σ) of the signal intensity, was calculated in the background (BG) delineated by with a yellow circle (Fig. 1b), and integrated in: $SNR = 0.655.\frac{m_{RL}}{\sigma_{BG}}$ where the factor 0.655 corrects the standard equation to account for the Rician rather than Gaussian distribution of the background signal (Yu et al. 2019). The quality of the phase image was assessed using stiffness confidence images (Fig. 1c) generated with MRE-Lab software (Mayo Clinic, USA). The red contour was duplicated from the magnitude image, and the mean stiffness confidence (SC) level and the stiffness area with a confidence level higher than 0.95 (AHC) were then calculated.

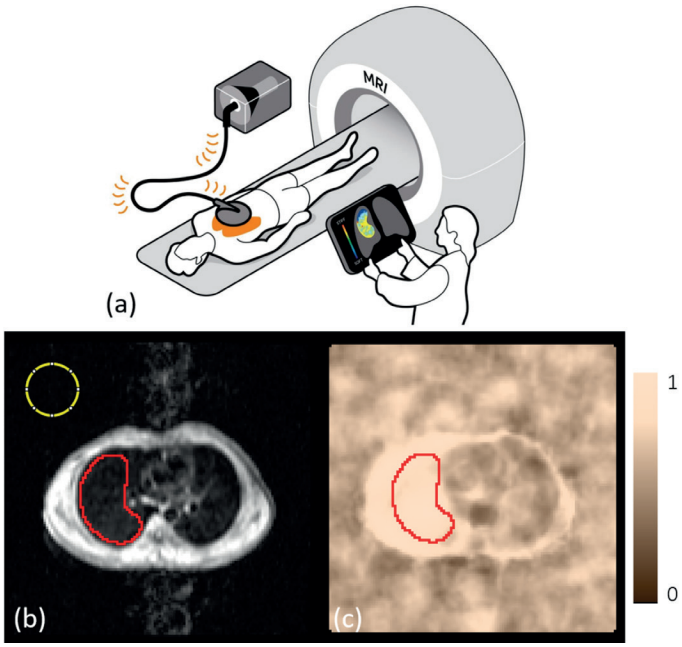

Figure 1. Set-up (a), outlines of the lung (red contour) and background (yellow circle) regions in MR magnitude (b) and stiffness confidence maps (c).

2.3 Statistical analysis

The values of SNR, SC and AHC were expressed in mean and standard deviation, and compared between the four slices using two-sample Wilcoxon-Mann-Whitney test.

3. Results and discussion

Table 1 shows that the SNR data are not statistically different between slices, with a value of around 4. This result indicates that the magnitude images have sufficient signal amplitude (4 times higher than the noise) regardless of the selected slice among the four.

However, the stiffness confidence (SC) level and the area of high confidence (AHC) are statistically different ($P < 0.001$) when comparing the value on slice 1 or 2 with those on slice 3 or 4.

Table 1. Comparison of image quality parameters in the right lung region of 34 smokers (mean ± SD)

	SNR	SC	AHC
Slice 1	4.16±1.07	0.72±0.10	1.9±7.0
Slice 2	3.95±0.89	0.69±0.10	1.3±6.8
Slice 3	4.13±1.04	0.87±0.09	23.1±25.2
Slice 4	4.25±1.14	0.85±0.09	19.5±23.2
All 4 slices	4.18±0.95	0.79±0.07	11.8±0.1

SNR: signal-to-noise ratio; SC: stiffness confidence; AHC: area (%) of high confidence level (> 0.95).

The measurement obtained for SC and AHC parameters revealed that lung stiffness is more accurately estimated on slices 3 and 4, which correspond to the lower regions of the right lung. In contrast, the phase difference measured by MRE in the upper slices may be less reliable due to the reflections of the mechanical wave on the ribs of the thoracic cage. As a result, lung stiffness values are likely more impacted by phase difference measurement in the upper lung slices.

4. Conclusions

This study has demonstrated the good quality of the images produced by the MRE lung tests. Furthermore, the analysis has provided valuable insights for reducing scan time. Specifically, lung stiffness could be reliably assessed using only the two lower slices, instead of the current four, thereby improving the confidence level in stiffness measurements while streamlining the procedure. In perspective, the MRE protocol could be improved by generating shear waves in right and left lungs.

Conflict of Interest Statement

None.

Contributor Roles

PP: Software, Methodology, Writing original draft; SFB: Methodology, Writing original draft; Supervision,

Funding acquisition, Validation, Writing-review & editing; FC: Validation, Writing-review & editing.

Funding

This project was co-founded by the European Union through the European Regional Development Fund (FEDER/ERDF) within the framework of the Contrat de Plan Etat-Région (CPER) tecsante 2021–2027 for the Hauts-de-France region.

References

Bensamoun, S. F., McGee, K. P., Chakouch, M., Pouletaut, P., & Charleux, F. (2025a). Monitoring of lung stiffness for long-COVID patients using magnetic resonance elastography (MRE). *Magnetic Resonance Imaging, 115*, 110269. https://doi.org/10.1016/j.mri.2024.110269

Bensamoun, S.F., McGee, K., Chakouch, M., Pouletaut, P., & Charleux, F. (2025b). Quantification of Lung Stiffness Using Magnetic Resonance Elastography (MRE): Clinical Validation for Smokers. *IEEE Transactions on Biomedical Engineering, 72*(9), 2851–2858. https://doi.org/10.1109/TBME.2025.3553375

Chakouch, M. K., Pouletaut, P., Charleux, F., Bensamoun, S. F. (2023). How magnetic resonance elastography (MRE) could provide biomechanical properties to complete computed tomography (CT) scan lung diagnostic? 48th Congress of the Society of Biomechanics. *Computer Methods in Biomechanics and Biomedical Engineering, 26* (sup1), S128. https://doi.org/10.1080/10255842.2023.2246304

Silva, A. M., Grimm, R. C., Glaser, K. J., Fu, Y., Wu, T., Ehman, R. L., & Silva, A. C. (2015). Magnetic resonance elastography: evaluation of new inversion algorithm and quantitative analysis method. *Abdominal imaging, 40*, 810–817. https://doi.org/10.1007/s00261-015-0372-5

Yu, S., Dai, G., Wang, Z., Li, L., Wei, X., & Xie, Y. (2018). A consistency evaluation of signal-to-noise ratio in the quality assessment of human brain magnetic resonance images. *BMC Medical Imaging, 18*, 1–9. https://doi.org/10.1186/s12880-018-0256-6

2025-2 | 50th congress of the Société de Biomécanique
27-29 October 2025, Marseille, France

Multidisciplinary Biomechanics Journal

A combined modeling and AI-driven optimization approach to enhance surfactant replacement therapy in adult lungs

Philippe Meliga*, Gregor Roncin, Elie Hachem

Mines Paris, PSL University, Centre for material forming (CEMEF), UMR CNRS, 06904 Sophia Antipolis, France
* Corresponding author: philippe.meliga@mines-paristech.fr

Received date: 04/04/2025
Accepted date: 27/06/2025
Publication date: 27/10/2025

Keywords: respiratory distress syndrome, surfactant replacement therapy, pulmonary drug delivery, biological fluid mechanics, deep reinforcement learning

© 2025 The Authors
Licence CC-BY 4.0
Published by Société de Biomécanique

1. Introduction

Surfactant Replacement Therapy (SRT) is a life-saving treatment for neonatal respiratory distress syndrome (NRDS), a condition where surfactant deficiency causes alveolar collapse and respiratory failure. SRT has proven highly effective in preterm infants, but remains largely ineffective in adults, particularly in acute respiratory distress syndrome (ARDS), where current surfactant administration strategies fail to achieve sufficient alveolar delivery. Anatomical and physiological differences account for this discrepancy: adult bronchial trees are larger, which result in higher surfactant deposition on airway walls and decreased alveolar delivery. Despite advances in respiratory medicine, current protocols remain poorly suited to address the unique challenges of adult lung anatomy, highlighting the need for customized administration strategies.

2. Methods

To address these challenges, our study presents a computational framework that integrates an advanced mathematical model of surfactant delivery with machine learning (ML) techniques. The model follows a two-step propagation process: initially, a liquid plug spreads down the airway tube, coating the walls and flowing along the bronchial pathways. At each bifurcation, the plug splits, redistributing the surfactant throughout the bronchial tree in a recursive manner. This approach builds upon the foundational work of Filoche et al. 2015, incorporating asymptotic analyses where inertial and capillary forces dominate. By leveraging these principles, the model predicts surfactant delivery efficiency and homogeneity under a variety of conditions, ranging from neonatal to adult lung geometries. To systematically explore the impact of lung size and airway complexity, bronchial tree models of varying dimensions were generated, parameterized by tracheal diameter, and extended up to 15 generations. This allows for a comprehensive assessment of size and truncation effects. The model also accounts for clinically relevant parameters, including surfactant viscosity (with Curosurf as a reference), dose volumes, flow rates, and patient positioning. For optimization, we coupled this model with an in-house Deep Reinforcement Learning (DRL) algorithm. This AI-based approach enables thorough exploration of complex parameter spaces, as demonstrated by Hachem et al. 2021, which allows identifying robust administration protocols that adapt to variations in anatomy and fluid dynamics.

3. Results and discussion

Our findings reaffirm that, under classical administration conditions, the efficiency of surfactant delivery is significantly compromised in larger adult lungs due to excessive loss from airway coating, as initially reported in Kazemi et al. 2019. This results in poor alveolar deposition, reducing the therapeutic benefits of SRT in ARDS patients.

To cite this article: Philippe Meliga, Gregor Roncin, Elie Hachem, A combined modeling and AI-driven optimization approach to enhance surfactant replacement therapy in adult lungs, *Multidisciplinary Biomechanics Journal*, 2025, vol. 2, p. 135–137, DOI: 10.46298/mbj.16135.

We conducted extensive optimization runs under different constraints, evaluating both fixed-mixture conditions and free-mixture configurations to assess their respective impacts on delivery efficiency (Fig. 1).

Notably, our findings indicate that increasing the number of instillations does not necessarily enhance alveolar delivery. In fact, optimal surfactant distribution may be achieved by adjusting the instillation strategy; for example, delivering a fixed total dose in two aliquots instead of one or three can significantly improve alveolar deposition. This underscores the importance of not only optimizing total dosage but also fine-tuning delivery timing and distribution protocols to enhance therapeutic outcomes.

Our results demonstrate that combining detailed mathematical modeling with ML-based optimization can yield valuable insights into the fluid dynamics of SRT in larger lungs. As part of our ongoing efforts to refine this framework, we are now incorporating temporal dynamics into our simulations. By introducing time-dependent variables, we aim to design adaptive administration protocols that dynamically adjust in real time. These adaptive strategies leverage full actuation capabilities, allowing for modifications in patient positioning and real-time flow rate adjustments throughout the treatment. Such refinements maximize alveolar coating while simultaneously minimizing airway deposition, thereby improving overall delivery efficiency.

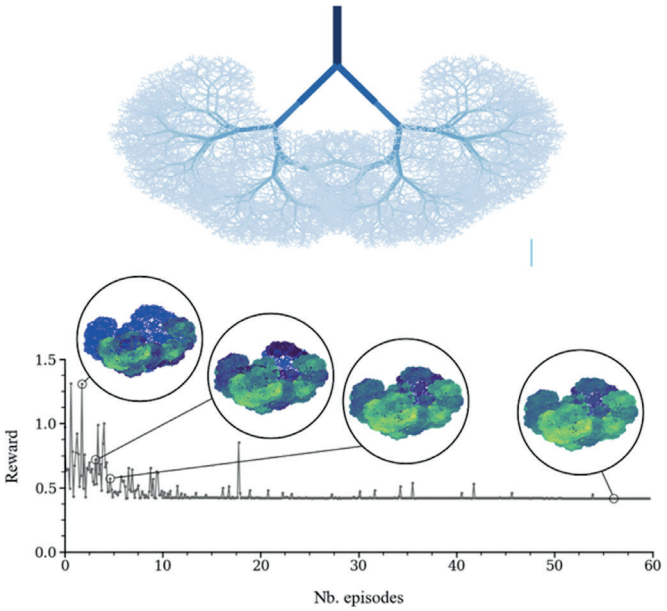

Figure 1. Top. Symmetric adult airway tree with 15 generations and 32,768 terminal branches. Airway narrowing is encoded by branch color and thickness.

Bottom. DRL optimization of surfactant delivery homogeneity by tuning instillation conditions and fluid rheology. The reward curve tracks progress over episodes (lower is better), with insets showing color-coded surfactant distributions at key stages of training.

Credit: G. Roncin

4. Conclusions

These advances are particularly significant given the limitations of traditional optimization methods in capturing the complex interplay of parameters governing surfactant delivery in large airways. In contrast, AI-driven strategies offer a powerful and individualized approach to protocol design. Our work marks a critical step toward personalized SRT, with potential impact on ARDS treatment and the extension of surfactant therapy beyond neonates.

To assess translational potential, experimental validation is underway in collaboration with clinical partners. The protocol will be tested in 3D-printed transparent airway models—ranging from simplified geometries with variable generation sizes to patient-specific anatomies—using programmable flow pumps and high-speed imaging to track fluid–air interface dynamics. These setups will enable direct comparison between standard clinical postures and DRL-optimized conditions under physiologically realistic flow scenarios.

Conflict of Interest Statement

None.

Contributor Roles

PM: Conceptualization, Methodology, Funding acquisition, Project administration, Supervision, Writing original draft; GR: Data curation, Formal analysis, Investigation, Validation, Visualization & editing; EH: Conceptualization, Funding acquisition, Resources, Supervision, Writing-review & editing.

Funding

This research was funded by the French National Research Agency (ANR) under the project ANR-23-CE45-0009-01.

References

Filoche, M., Tai, C.-F., & Grotberg, J. B. (2015). Three-dimensional model of surfactant replacement

therapy. *Proc. Natl. Acad. Sci. U. S. A., 112*(30), 9287-9292. https://doi.org/10.1073/pnas.1504025112

Hachem, E., Ghraieb, H., Larcher, A., Viquerat, J., & Meliga, P. (2021). Deep reinforcement learning for the control of conjugate heat transfer. *J. Comp. Phys., 436*, 110317. https://doi.org/10.1016/j.jcp.2021.110317

Kazemi, A., Louis, B., Isabey, D., Nieman, G. F., Gatto, L. A., Satalin, J., Baker, S. Grotberg, J. B., & Filoche, M. (2019). Surfactant delivery in rat lungs: Comparing 3D geometrical simulation model with experimental instillation. *PLoS Comput. Biol., 15*(10), e1007408. https://doi.org/10.1371/journal.pcbi.1007408

2025-2 | 50th congress of the Société de Biomécanique
27-29 October 2025, Marseille, France

Multidisciplinary Biomechanics Journal

The role of lingual frenulum on tongue mobility: a biomechanical modeling study

Maëlle Courtin[a], Yohan Payan[a], Pascal Perrier[b], Morgane Evin[c], Emilie Clady[d], Pierre Frémondière[d, e], Mohammad Ali Nazari[f], Maxime Calka[b*]

a Univ. Grenoble-Alpes, CNRS, Grenoble INP, TIMC, F-38000 Grenoble, France
b Univ. Grenoble-Alpes, CNRS, Grenoble INP, GIPSA-Lab, F-38000 Grenoble, France
c Univ. Aix-Marseille, iLab Spine, F-13000, Marseille, France
d École universitaire de Maïeutique Marseille, France
e ADES UMR 7268 Aix Marseille Univ, Marseille, France
f School of Mechanical Engineering, University of Tehran, Tehran, Iran
* Corresponding author: maxime.calka@univ-grenoble-alpes.fr

Received date: 04/04/2025
Accepted date: 27/06/2025
Publication date: 27/10/2025

Keywords: biomechanical FE models, baby tongue, frenulum, frenectomy, ankyloglossia

© 2025 The Authors
Licence CC-BY 4.0
Published by Société de Biomécanique

1. Introduction

Ankyloglossia, or tongue-tie, is a condition that limits tongue mobility and affects around 3% of infants, often making breastfeeding difficult. The lingual frenulum is seen as a key factor in this disorder. Since the early 2000s, the number of frenotomies—surgical cuts of the frenulum—has increased significantly, despite ongoing debates about their effectiveness and the lack of long-term data (Sawai et al., 2024).

To better understand the impact of the lingual frenulum on tongue mobility during breastfeeding and evaluate treatment options, the TongueTieNum project aims to develop a biomechanical finite element (FE) model of a newborn's tongue. This model simulates the tongue's mechanical interactions with the mother's nipple to estimate the tongue's pressure on the nipple depending on the frenulum's morphology and mechanical properties. The objective of this preliminary study is to quantify the influence of the frenulum on the pressure that the tongue can exert on the nipple.

2. Methods

2.1 Generation of the FE newborn tongue model

The FE newborn tongue model was generated starting from a model that represents the tongue of a French male called "Reference Subject" (bmi of 20 kg/m^2, aged 60), using a 3D non-rigid landmark-based volume image registration method (Bijar et al., 2016) between MRI 3D views of the heads of the Reference Subject (RS) and of a newborn. The optimal transformation between the 2 MR image sets was applied to the RS FE tongue model (Calka et al., 2025) in order to transform its morphology into the one of the newborn tongue.

2.2 Nipple modelling

As a first step, a rough model of the nipple was generated (Figure 1 – panel d), which consists of a deformable cylinder of 24 mm in diameter and 35 mm long (Alatalo et al., 2019). In a first approximation the nipple was assumed to have the same material properties as the tongue. Standard mechanical contacts were defined between the tongue, from the tip to the blade, and the lowest part of the cylinder that represents the nipple.

2.3 Studying tongue mobility: a sensitivity study

Simulations were carried out to determine the impact of the frenulum's morphological and mechanical characteristics on tongue mobility for a gesture that simulates tongue movement during breastfeeding. In these simulations, the front part of tongue was raised by the activation of the superior longitudinalis (SL) muscle. This elevation induced an increase of tongue pressure on the nipple. A sensitivity study was carried out on 3 characteristics of the frenulum (F): morphology, thickness and stiffness. Three morphologies were considered according to the proximity of the frenulum's insertion relative to the tongue tip (Figure 1 – panel c): posterior (P), median (M), anterior (A). Two thicknesses (T) were

To cite this article: Maëlle Courtin, Yohan Payan, Pascal Perrier, Morgane Evin, Emilie Clady, Pierre Frémondière, Mohammad Ali Nazari, Maxime Calka, The role of lingual frenulum on tongue mobility: a biomechanical modeling study, *Multidisciplinary Biomechanics Journal*, 2025, vol. 2, p. 385–387, DOI: 10.46298/mbj.16257.

tested: 1 mm and 3 mm. Stiffness (S) was defined based the value proposed by Souiki et al., 2025 (this conference), considering ratio of 1 or 3 with regard to the rigidity of the tongue (Yeoh 2 parameters, C1=192Pa, C2=90Pa). Thus, 12 simulations were carried out that were referenced as F-(P, M, A) T-(1, 3) S-(1, 3).

3. Results and discussion

3.1 FE newborn model

The FE newborn model is shown in Figure 1. The registration process enabled us to obtain an accurate morphology that fits well to the MRI ground truth.

3.2 Sensitivity study of the tongue frenulum

The simulations show that the most important property is the position of the frenulum used. For each position, Table 1 lists the mean and the standard deviation of the tongue pressure exerted on the cylinder representing the nipple, together with the maximum pressure (4 simulations for each position with various T and S).

Table 1. Mean and standard deviation of the pressures exerted by the tongue against the cylinder that represents the nipple for each frenulum position tested.

	Mean (Pa)	SD (Pa)	Max (Pa)
F-P	123.7	1.7	224
F-M	87.5	4.9	186
F-A	75.5	11.7	178

These preliminary results show that an anterior frenulum is more restrictive than a posterior one, supporting the idea that ankyloglossia results from an overly forward frenulum that limits tongue mobility, especially its elevation toward the palate in newborns. In addition, low standard deviation shows that thickness and stiffness parameters have little influence for posterior tongue frenulum, but much more for the anterior ones, with a maximum pressure of 178 Pa for the F-A T-3 S-3 simulation.

4. Conclusions

To conclude, this work presents the design of a FE newborn tongue model including an account of the tongue frenulum with the aim of carrying out a sensitivity study to characterize which parameters play major roles in the emergence of an ankyloglossia.

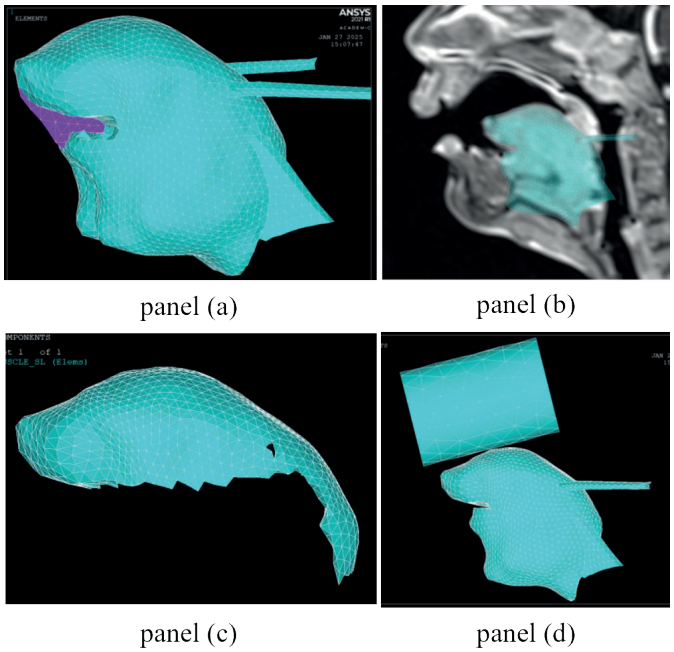

Figure 1. FE newborn model. Panel (a): FE newborn with anterior tongue frenulum (in violet). Panel (b): FE model superimposed on newborn MRI in the sagittal plane of the head. Panel (c): SL muscle. Panel (d): FE model with nipple model.

This work is preliminary and does not yet allow us to draw definitive conclusions about the role of the frenulum and its morphology in breastfeeding. However, it does offer a new approach based on biomechanical modeling that can further be used in research on breastfeeding and its impairments.

As a short-term perspective, the realism of the model will be improved by adding the mandible while sucking movements will be simulated using tongue muscle coactivation.

In the long term, this model could be coupled with the breast model developed within the TIMC laboratory (Mîra et al., 2018).

Conflict of Interest Statement

None.

Contributor Roles

Maëlle Courtin: Modeling, Methodology, Writing; Yohan Payan: Methodology, Writing, Supervision, Funding; Pascal Perrier: Methodology, Writing, Supervision; Morgane Evin: Methodology, Writing, Supervision, Project initiator; Emily Clady: Consulting, Writing; Pierre Frémondiere: Consulting, Writing;

Mohammad Ali Nazari: Modeling, Writing; Maxime Calka: Methodology, Writing, Supervision;

References

Alatalo, D., Jiang, L., Geddes, D., & Hassanipour, F. (2019). Nipple deformation and peripheral pressure on the arealo during breastfeeding. *Journal of Biomechanical Engineering*, 142(1), 011004. https://doi.org/10.1115/1.4043665

Bijar, A., Rohan, P. Y., Perrier, P., & Payan Y. (2016). Atlas-based automatic generation of subject-specific finite element tongue meshes. *Annals of Biomedical engineering, 44*, 16–34. https://doi.org/10.1007/s10439-015-1497-y

Calka, M., Badin, P., Nazari, M. A., Rochette, M., Perrier, P. et al. (2025). The G-OBIM tongue model: An accurate open-source biomechanical model of a male human tongue. *PLOS Computational Biology 21*(9), e1013378. https://doi.org/10.1371/journal.pcbi.1013378

Mîra, A., Carton, A. K., Muller, S., & Payan, Y. (2018). A biomechanical breast model evaluated with respect to MRI data collected in three different positions. *Clinical Biomechanics, 60*, 191–199. https://doi.org/10.1016/j.clinbiomech.2018.10.020

Sawai, A. C., Mahajani, M., Subhadarsanee, C., Patil, K., Dhadse, P. V., Sawai Jr, A. C., & Patil, K. S. (2024). Management of tongue-tie using conventional technique for speech clarity and correcting malocclusion: A case report. *Cureus*, 16(7). https://doi.org/10.7759/cureus.63756